

PARAMAGNETIC-RESONANCE STUDY OF THE DYNAMIC JAHN-TELLER EFFECT  
IN  $\text{CaF}_2:\text{Sc}^{2+}$  AND  $\text{SrF}_2:\text{Sc}^{2+}$

U. T. Höchli and T. L. Estle  
Texas Instruments Incorporated, Dallas, Texas  
(Received 5 December 1966)

$\text{Sc}^{2+}$  impurities in  $\text{CaF}_2$  and  $\text{SrF}_2$  are studied by electron paramagnetic resonance. The  $\text{Sc}^{2+}$  has an  $[\text{Ar}]3d^1$  configuration and undergoes a Jahn-Teller distortion. The vibronic states for the equivalent tetragonal distortions couple to give an inversion splitting of roughly  $10 \text{ cm}^{-1}$ .

This Letter reports the first observation of  $\text{Sc}^{2+}$  impurity ions by electron paramagnetic resonance (epr) and shows that the electron configuration is  $[\text{Ar}]3d^1$  for  $\text{Sc}^{2+}$  substitutional for the cation in  $\text{CaF}_2$  and  $\text{SrF}_2$ . The  $\text{ScF}_8$  complex distorts as a result of the Jahn-Teller effect.<sup>1</sup> The types of spectra and the temperature range in which they are observed are explained in terms of the occupation of states of the complex. The states of lowest energy arise from coupling of the vibronic states corresponding to the equivalent distortions of the complex, those of higher energy are rotational-like. Both are a consequence of the dynamic Jahn-Teller effects.

Epr data have been taken on Sc-doped single crystals of  $\text{CaF}_2$  and  $\text{SrF}_2$  which were x irradiated at room temperature. At  $1.5^\circ\text{K}$  and  $9.2 \text{ GHz}$  with the magnetic field parallel to a  $\langle 111 \rangle$  axis, a single eight-line hyperfine pattern with a splitting of about  $60 \text{ G}$  is observed

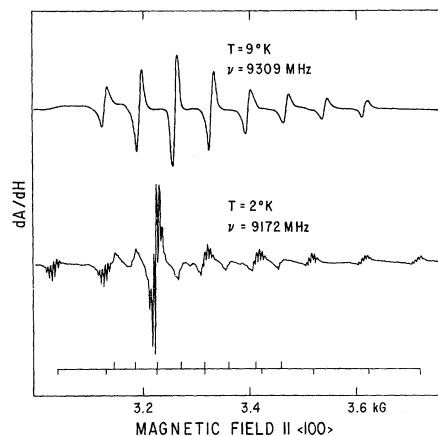


FIG. 1. Epr spectra of  $\text{CaF}_2:\text{Sc}^{2+}$  with  $\vec{H} \parallel \langle 100 \rangle$ . Derivative of absorption versus magnetic field expressed in terms of proton resonance frequency. Above: the isotropic spectrum of the  $\Gamma_8$  state. Below: the two anisotropic spectra of the  $\Gamma_8$  state. The positions of the hyperfine lines are indicated by the bar graph at the bottom of the figure.

resulting from interaction with the  $\text{Sc}^{45}$  nucleus ( $I = \frac{7}{2}$ , abundance = 100%). Each hyperfine line is further split into nine superhyperfine components which have a splitting of  $2.2 \text{ G}$  and an intensity distribution of about 1:8:28:56:70:56:28:8:1, indicative of an interaction with eight equivalent  $\text{F}^{19}$  nuclei ( $I = \frac{1}{2}$ , abundance = 100%) as expected of isolated  $\text{Sc}^{2+}$  substitutional for  $\text{Ca}^{2+}$  or  $\text{Sr}^{2+}$ .

For arbitrary orientations three different types of spectra are observed in three different temperature ranges. Between  $1.5$  and  $5^\circ\text{K}$ , two anisotropic cubic spectra are observed, as shown in Fig. 1. The angular dependence of the effective  $g$  factors is shown in Fig. 2 and has the form

$$g = g_1 \pm g_2 [1 - 3(l^2 m^2 + m^2 n^2 + n^2 l^2)]^{1/2}, \quad (1)$$

where  $l$ ,  $m$ , and  $n$  are the direction cosines of the magnetic field,  $\vec{H}$ , with respect to the cubic axes of the crystal. The effective hyperfine splitting parameter,  $K$ , also fits Eq. (1). The values of  $g$  and  $K$  for  $\vec{H}$  along  $\langle 100 \rangle$  are given in Table I.

In the temperature range between  $5$  and about  $30^\circ\text{K}$ , an isotropic spectrum is observed (see Fig. 1). Its parameters, also listed in Table I, are an average of the parameters determined

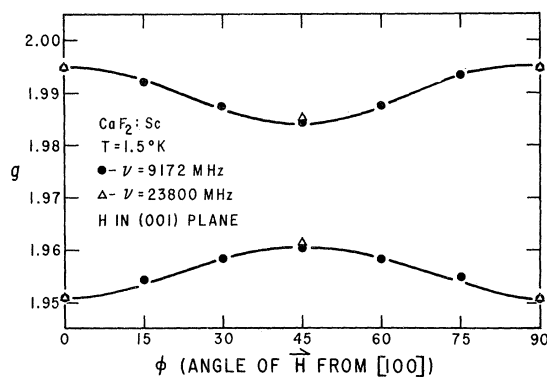


FIG. 2. The  $g$  factors of the anisotropic spectra.

Table I. The  $g$  factors and hyperfine constants,  $K$ , for  $\text{CaF}_2:\text{Sc}$  and  $\text{SrF}_2:\text{Sc}$ ,  $\vec{H} \parallel \langle 100 \rangle$ .

	$\text{CaF}_2:\text{Sc}$		$\text{SrF}_2:\text{Sc}$	
	$g^a$	$K^b$	$g^a$	$K^b$
$\Gamma_8$	1.951	89.5	1.936	91.2
	1.995	40.4	1.991	43.0
$\Gamma_6$	1.969	65.5	1.963	67.0
rot.	1.967	65.0	not observed	not observed

<sup>a</sup>The accuracy of the  $g$  factors is  $10^{-3}$  or better.

<sup>b</sup>Hyperfine constants are given in units of  $10^{-4} \text{ cm}^{-1}$  with an accuracy of  $0.5 \times 10^{-4} \text{ cm}^{-1}$ .

for the low-temperature spectrum for  $\vec{H}$  along  $\langle 100 \rangle$ . The intensity,  $I$ , of this spectrum satisfies

$$I \propto \{T[2 \exp(\Delta/kT) + 1]\}^{-1}, \quad (2)$$

where  $\Delta \approx 10 \text{ cm}^{-1}$  for  $\text{CaF}_2:\text{Sc}$  and  $\Delta \approx 8 \text{ cm}^{-1}$  for  $\text{SrF}_2:\text{Sc}$ . At these temperatures the anisotropic spectra have broadened beyond detection. The anisotropic and isotropic spectra have similar nonuniform amplitude and width distributions. Above  $30^\circ\text{K}$  another isotropic spectrum (see Table I) is observed which is described by parameters almost identical to those used for the first isotropic spectrum. However, the amplitude distribution is uniform. This spectrum broadens from  $50$  to  $80^\circ\text{K}$  with the relaxation time, determined through line broadening, proportional to  $\exp(\delta/kT)$  ( $\delta = 250 \pm 50 \text{ cm}^{-1}$  for  $\text{CaF}_2$  and somewhat less for  $\text{SrF}_2$ ).

A  $\text{Sc}^{2+}$  ion with an  $[\text{Ar}]3d^1$  configuration has a  ${}^2\Gamma_3$  ground state in the  $O_h$  symmetry of the cation site of the  $\text{CaF}_2$  lattice. Such an ionic complex is unstable against a tetragonal distortion.<sup>1</sup> The vibronic states for each distortion are coupled because of the low barrier,<sup>2</sup> a process sometimes referred to as tunneling. The weak coupling limit leads to the well-known static Jahn-Teller effect. For coupling comparable with or greater than the anisotropy of the Zeeman terms, such as is the case here, the vibronic states are coupled to give an excited singlet state and a doublet ground state.<sup>3</sup> With spin these become a  $\Gamma_6$  doublet and a  $\Gamma_8$  quartet, respectively. The energy parameter  $\Delta$  in Eq. (2) is called the inversion splitting<sup>4</sup> and is the energy difference between the  $\Gamma_8$  and  $\Gamma_6$  states. The temperature dependence of the spectrum up to  $30^\circ\text{K}$  results from the occupancy and relaxation of these two states.

For an inversion splitting large compared

with the anisotropy of the Zeeman interaction, and the interaction with static strains, the Zeeman effect for the  $\Gamma_6$  and  $\Gamma_8$  states can be calculated separately. This together with a small Zeeman anisotropy is sufficient to produce an isotropic  $\Gamma_6$ -state epr spectrum and to give an anisotropy to the  $\Gamma_8$ -state epr spectrum of the form shown in Eq. (1). An extension of the treatment of Bersuker<sup>5</sup> and Coffman,<sup>6</sup> who considered the coupling of  $t_{2g}$  orbitals into the lower  $e_g$  orbitals via the spin-orbit interaction, leads to the expressions  $g_1 = 2 + 4\lambda/10Dq$  and  $g_2 = 2\lambda(1 + \frac{3}{2}\gamma)/10Dq$ , where  $\lambda$  is the spin-orbit interaction constant,  $10Dq$  is the  $e_g$ -to- $t_{2g}$  splitting, and  $\gamma$  is the vibrational overlap. Comparison with our results for  $\text{CaF}_2:\text{Sc}$  gives  $\lambda/10Dq = 0.0074$  and  $\gamma = 0.24$ . Such moderate-coupling theories need modification when extended to large overlap and applied to strain or Zeeman interaction between states of different symmetry.

The uniform isotropic spectrum observed above  $30^\circ\text{K}$  results from the occupation of rotational-like excited states. At still higher temperatures this spectrum broadens<sup>7</sup> because of Orbach relaxation to states higher in energy by  $\delta$ . The large hyperfine anisotropy suggests more complex angular dependence of the  $\Gamma_8$  hyperfine spectrum than Eq. (1). The observed hyperfine splitting which fits Eq. (1) is not understood and may represent a good test of any proposed theory. The nonuniform width and intensity distributions of the  $\Gamma_8$  and  $\Gamma_6$  epr spectra may arise from the coupling of these two states via random internal strains although no consistent description has yet been obtained.

The authors wish to acknowledge the valuable contributions of W. C. Holton and M. de Wit.

†Work supported in part by U. S. Air Force Office of Scientific Research Contract No. AF49(638)-1250.

<sup>1</sup>H. A. Jahn and E. Teller, Proc. Roy. Soc. (London) **161**, 200 (1937). See also C. J. Ballhausen, Introduction to Ligand Field Theory (McGraw-Hill Book Company, Inc., New York, 1962), pp. 193-207.

<sup>2</sup>The barrier arises from cubic terms in the Hamiltonian for interaction between electronic and nuclear degrees of freedom [see M. C. M. O'Brien, Proc. Roy. Soc. (London) **A281**, 323 (1964)].

<sup>3</sup>The symmetric state is higher in energy because of the negative overlap of the electronic functions.

<sup>4</sup>The term inversion splitting is used by analogy with the similar phenomenon in the  $\text{NH}_3$  molecule [see, for

example, C. H. Townes and A. L. Schawlow, *Micro-wave Spectroscopy* (McGraw-Hill Book Company, Inc., New York, 1955), Chap. 12]. Similar behavior is also observed for paraelectric and paraelastic defects in crystals [see, for example, P. Sauer, O. Schirmer, and J. Schneider, *Phys. Status Solidi* **16**, 79 (1966)].

<sup>5</sup>I. B. Bersuker, S. S. Budnikov, B. G. Vekhter, and B. I. Chinik, *Fiz. Tverd. Tela* **6**, 2583 (1964) [transla-

tion: *Soviet Phys.—Solid State* **6**, 2059 (1965)], and references therein.

<sup>6</sup>R. E. Coffman, *Phys. Letters* **19**, 475 (1965); **21**, 381 (1965). Coffman reports that the part of the  $\text{Cu}^{2+}$  spectrum in MgO which can be resolved shows the characteristic angular dependence for a  $\Gamma_8$  state.

<sup>7</sup>U. T. Höchli, K. A. Muller, and P. Wysling, *Phys. Letters* **15**, 5 (1965).

### $\text{Ar}^{40}(d, p)$ EXCITATION FUNCTIONS OVER THE GROUND-STATE ISOBARIC ANALOG ENERGY REGION\*

P. Wilhjelm

University of North Carolina, Chapel Hill, North Carolina, and Duke University, Durham, North Carolina

and

G. A. Keyworth, G. C. Kyker, Jr., D. L. Sellin, N. R. Roberson, and E. G. Bilpuch

Duke University, Durham, North Carolina

(Received 21 December 1966)

In a recent experiment reported by Moore et al.,<sup>1</sup> an anomalous behavior of the excitation function of the reaction  $\text{Zr}^{90}(d, p)\text{Zr}^{91}$  was found. These anomalies occurred at incident deuteron energies corresponding to formation through the  $(d, n)$  channel of the  $T_{>}$  states of  $\text{Nb}^{91}$  whose parent analogs are the ground and first excited states of  $\text{Zr}^{91}$ . The de-excitation proton yield for the  $(d, np)$  reaction was also found to rise sharply in the vicinity of the first anomaly. These anomalies were interpreted as giving evidence for strong coupling between the analog  $(\text{Zr} + p)$  and  $(\text{Nb} + n)$  channels.

Following a suggestion by Moore, we have investigated the possibility of a similar effect in the reaction  $\text{Ar}^{40}(d, p)\text{Ar}^{41}$ . This target is of interest as the analogs in  $\text{K}^{41}$  of some of the low-lying states of  $\text{Ar}^{41}$  are known, from high-resolution measurements at this laboratory,<sup>2</sup> to exhibit fine structure.

According to the Coulomb energy difference of  $6.87 \pm 0.04$  MeV found in Ref. 2, the threshold for excitation of the isobaric analog of the ground state of  $\text{Ar}^{41}$  through the reaction  $\text{Ar}^{40}(d, n)\text{K}^{41}$  should occur at  $2.86 \pm 0.04$  MeV. We have measured excitation functions from 2.5 to 3.1 MeV for eight of the stronger proton groups shown in Fig. 1 whose  $l_n$  values are given in Table I. The data were taken using an on-line DDP-224 computer. The cryogenic gas-target chamber and energy control system for the 3-MeV electrostatic generator have been described elsewhere.<sup>2</sup> Yield curves were taken in steps of 10 keV at a laboratory angle of  $135^\circ$

and with an average beam through the gas target of 30  $\mu\text{A}$ . In order to concentrate initially on the gross-structure effects, we accurately adjusted the energy at each point and then swept the beam energy by  $\pm 5$  keV. This was accomplished by sweeping the field in the beam-analyzing magnet by the appropriate amount. The curves in Fig. 2 were additionally smoothed by performing a three-point running average. The error bars indicated are computed for the three-point sum and not for the individual count. Because of fluctuations in the effective target density resulting from geometric difficulties, normalization was accomplished by dividing the proton count at each point by the  $\text{Ar}^{40}(d,$

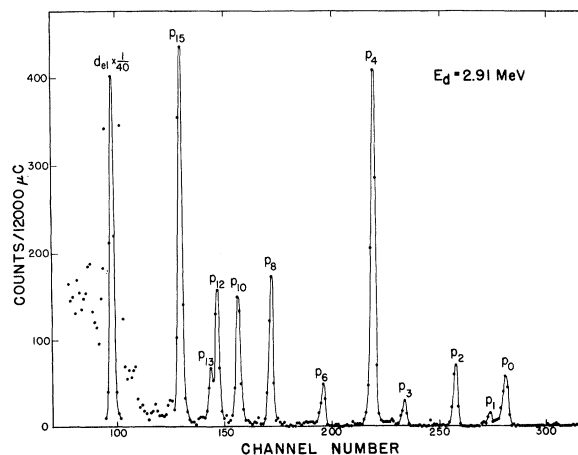


FIG. 1. A typical spectrum for one of the measurements with energy sweep  $\pm 5$  keV.